Comparison of Nitroaldol Reaction Mechanisms Using Accurate Ab Initio Calculations

Deborah Zorn, Victor S.-Y. Lin, Marek Pruski, and Mark S. Gordon*

Ames Laboratory and Department of Chemistry, Iowa State University, Ames, Iowa 50011

Received: June 11, 2008; Revised Manuscript Received: July 11, 2008

In the nitroaldol reaction, condensation between a nitroalkane and an aldehyde yields a nitroalcohol that can undergo dehydration to yield a nitroalkene. Amine-functionalized, MCM-41-type mesoporous silica nanosphere (MSN) materials have been shown to selectively catalyze this reaction. Gas-phase reaction paths for the several competing mechanisms for the nitroaldol reaction have been mapped out using second-order perturbation theory (MP2). Improved relative energies were determined using singles and doubles coupled cluster theory with perturbative triples, CCSD(T). The mechanism in the absence of a catalyst was used to provide a baseline against which to assess the impact of the catalyst on both the mechanism and the related energetics. Catalyzed mechanisms can either pass through a nitroalcohol intermediate as in the classical mechanism or an imine intermediate.

I. Introduction

The classical nitroaldol (or Henry) reaction (Scheme 1) is a base-catalyzed reaction between a nitrostabilized carbanion and an aldehyde or ketone. The reaction product is a nitroalcohol, which can undergo elimination of water to give a nitroalkene product.[1,2] Mesoporous silica nanosphere (MSN) catalysts have been found to selectively catalyze the nitroaldol reaction.[3] These MSN catalysts have been synthesized by cocondensation of organosilane precursors and tetraorthosilane (TEOS) in order to immobilize multiple functional groups on the inside of the silica pores. A primary amine-functionalized group catalyzes the nitroaldol reaction, and secondary groups control the selectivity. The secondary groups are called "gate keepers" because they avert unwanted reactants from entering the catalyst pore by noncovalent (e.g., hydrophobic or hydrophilic) interactions.[3] In addition to their selectivity, advantages of these new MSN catalysts include their inert stationary phase, large surface area, and tunable pore size. A schematic of a multifunctionalized system is shown in Figure 1. In this example, the gatekeeper groups only allow reactant A to enter the functionalized pore, yielding product A selectively.

Demicheli et al.[4] proposed a mechanism, shown in Scheme 2, for the reaction of benzaldehyde with nitromethane in an amine-functionalized MSN catalyst yielding nitrostyrene. The first step in this mechanism is the condensation of the supported amine with benzaldehyde, yielding a supported imine. The deprotonated nitromethane nitronate anion $[(NO_2CH_2)^-]$ then adds to the carbon of the imine carbon−nitrogen double bond to give a β-nitroamine. In the final step β-scission gives nitrostyrene and regenerates the catalyst. The experimental evidence for this mechanism was derived from the FT-IR spectrum of the product, showing the formation of a C═N stretch, which disappeared upon further addition of nitromethane. This evidence cannot rule out the classical mechanism shown in Scheme 1, suggesting that further study of this system is necessary.

Computational chemistry can be particularly helpful in elucidating reaction mechanisms. In work reported by Lecea et al.[5] fourth-order perturbation theory (MP4) calculations excluding triples, MP4SDQ,[6] were performed on five model nitroaldol reactions to study the stereochemical control of the reactions. Lecea et al. only presented the barriers for the first step of the classical nitroaldol reaction: addition of the $(NO_2CH_2)^-$ and an

SCHEME 1: The Nitroaldol (Henry) Reaction

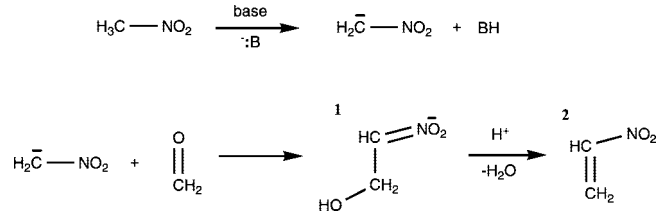

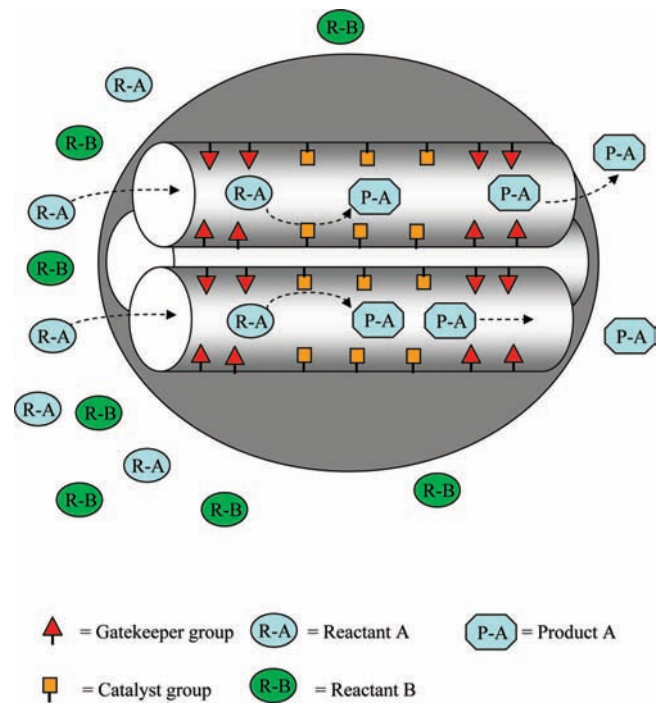

Figure 1. Schematic of a multifunctionalized mesoporous silica system.

* Corresponding author.

10.1021/jp805135p CCC: $40.75
Published on Web 09/30/2008

SCHEME 2: Proposed Mechanism for MSN-Catalyzed Nitroaldol Reaction[a]

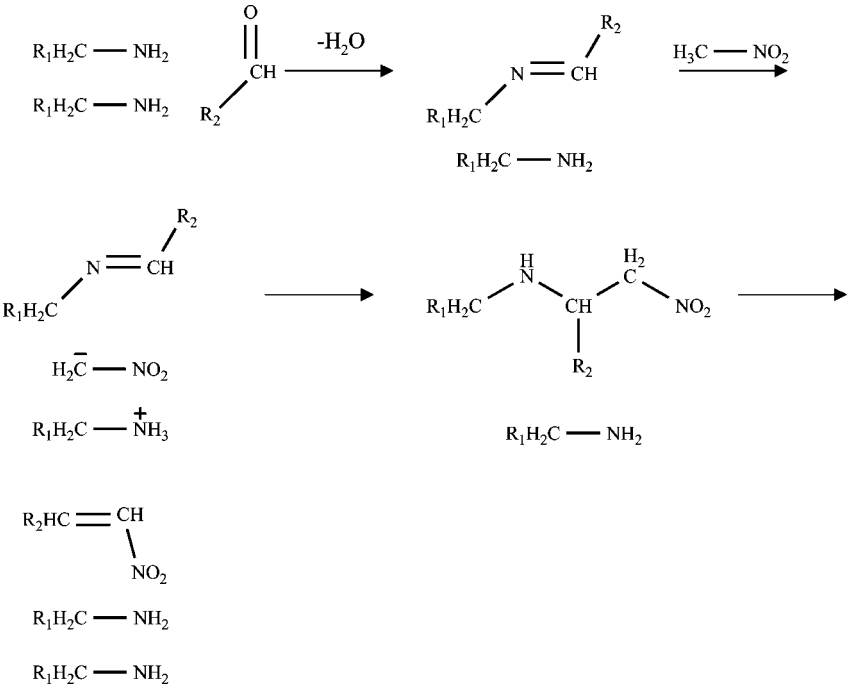

[a] $R_1 = (CH_2)_2$−MCM-41, R2 = C_6H_5.

SCHEME 3: Classical Mechanism with an Ab Initio Nitromethane Solvent Molecule

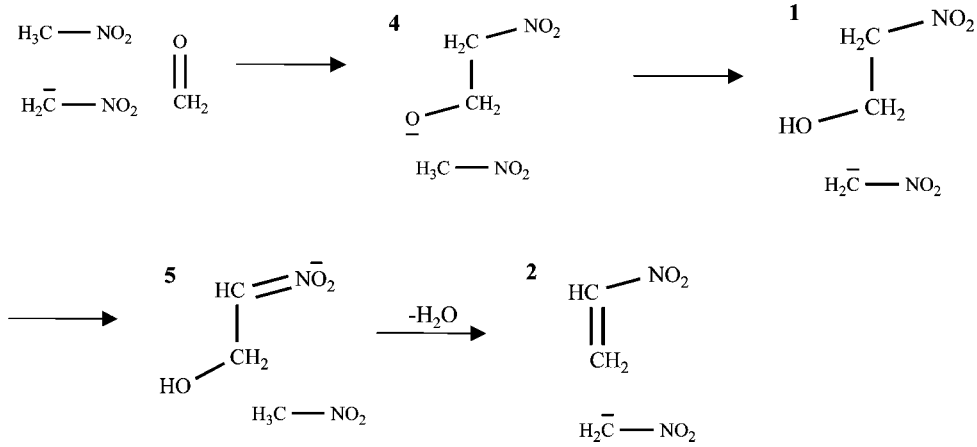

SCHEME 4: Mechanism of the Nitroaldol Reaction with an Amine Catalyst Molecule Present but Not Forming Covalent Bonds with the Reactants

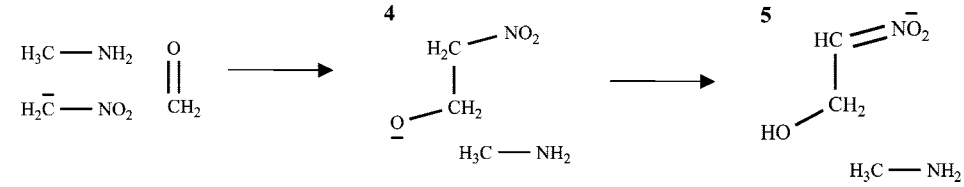

aldehyde. No barriers were given for subsequent steps such as the formation of the nitroalcohol and the dehydration reaction to give a nitroalkene.

The deprotonation of nitromethane by $(OH)^- \cdot nH_2O$ ($n = 0$, 2) clusters was studied by Beksic et al.[7] Hartree−Fock and second-order perturbation theory (MP2) calculations with the 6-31+G(d,p) basis set were performed to determine the geometries and energetics of the systems. The energy barrier for proton transfer from nitromethane to hydroxide with two waters was found to be only 4 kcal/mol above the reactant complex. The proton transfer reaction was found to be exothermic by 6.7 kcal/mol.

The catalyzed nitroaldol mechanism can proceed through an imine intermediate. Imine formation was studied with ab initio electronic structure calculations by Hall and Smith,[8] using the G-2(MP2,SVP) level of theory.[9] The barrier for carbinolamine formation was predicted to be 28.9 kcal/mol in the gas phase. With the addition of two water molecules, the formation of the carbinolamine proceeds via a zwitterionic intermediate, and the barrier is reduced to 3.5 kcal/mol. Imine formation without water

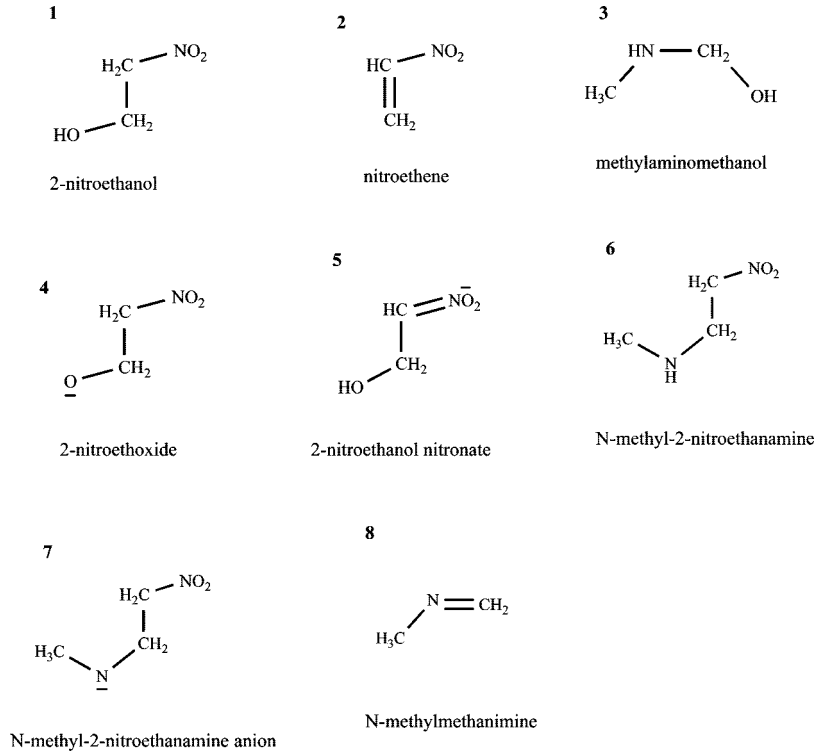

Figure 2. Summary of reaction intermediates and products shown in Schemes 1, 3, and 4.

SCHEME 5: Amine-Catalyzed Mechanisms[a]

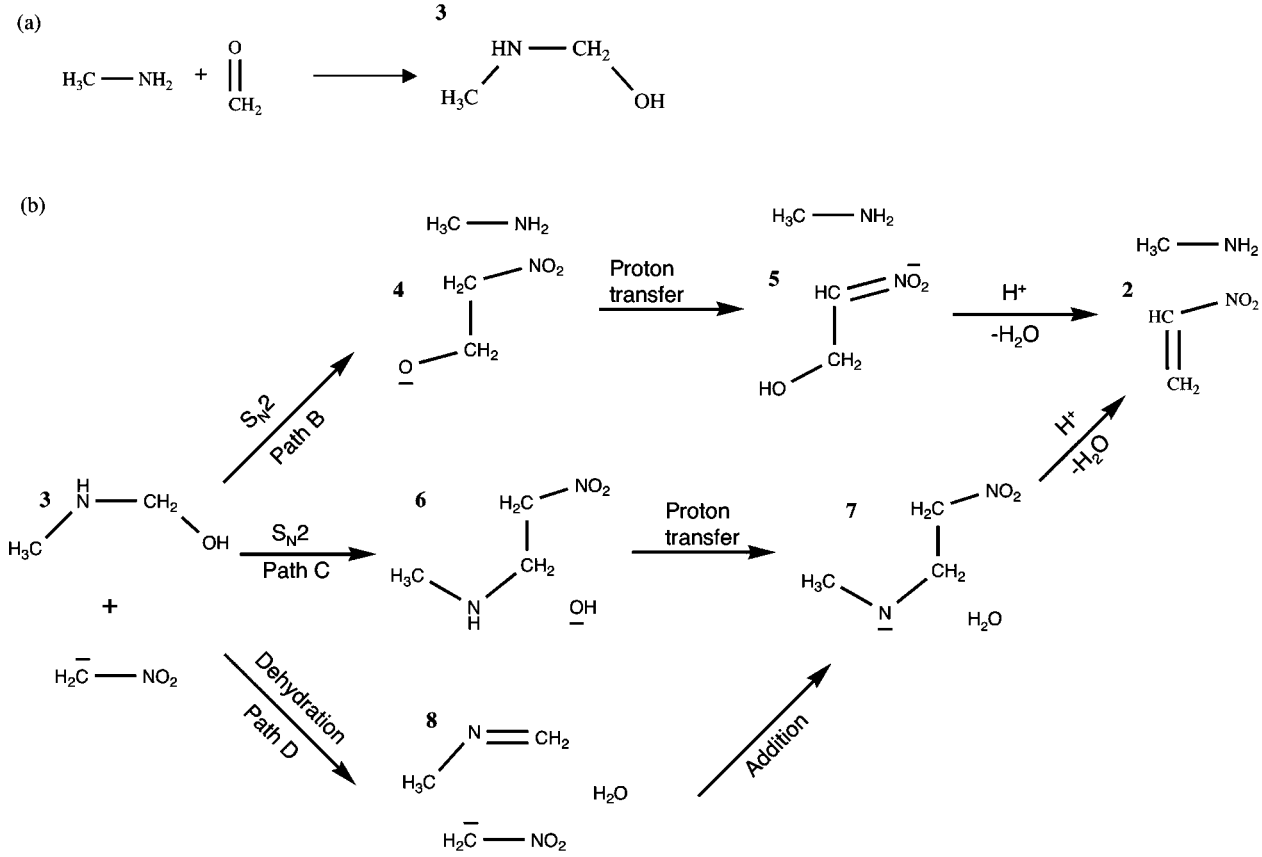

[a] (a) First step in the catalyzed mechanism: activation of formaldehyde by addition of amine; (b) paths B, C, and D.

proceeds by a four-center transition state, which is 55.3 kcal/mol higher in energy than the carbinolamine. Addition of one water lowers this barrier by 22.1 kcal/mol. Addition of a second waters lowers the barrier by an additional 6.5 to 26.7 kcal/mol. Aqueous free energies and acid−base equilibrium constants were also calculated.

The first step in understanding the mechanism for the amine-functionalized MSN-catalyzed reaction is to study the gas-phase

SCHEME 6: Catalyzed Mechanism Pathway D with an Additional Methylamine Molecule

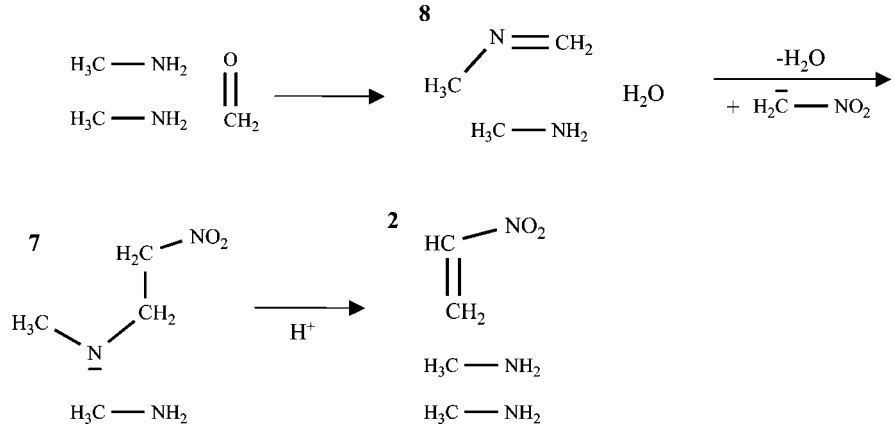

reactions. The present work will compare several possible mechanisms (see Schemes 4−6) for the amine-catalyzed nitroaldol reaction using accurate ab initio electronic structure calculations. These mechanisms will be discussed in detail in section III. Figure 2 summarizes most of the structures presented in Schemes 1, 3, 4, 5, and 6. The structure numbers (**1**−**8**) used throughout the text refer to the numbers given in Figure 2. The classical mechanism will be used as a baseline for comparison.

II. Computational Methods

Structures were obtained by performing gas-phase MP2 calculations,[10,11] using the 6-31+G(d) basis set.[12−15] Hessians (second-order derivatives of the energy) were used to characterize stationary points. Intrinsic reaction coordinate (IRC) calculations with the Gonzalez−Schlegel second-order method[16,17] were used to connect transition states with reactants and products.

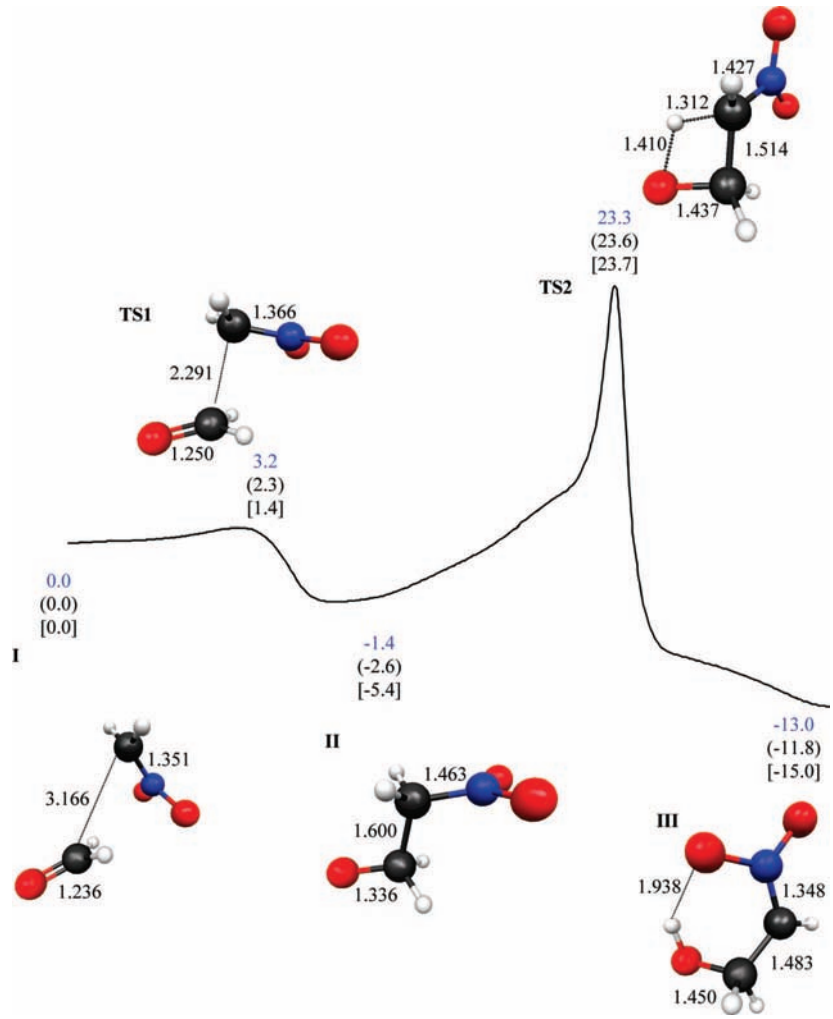

Figure 3. MP2/6-31+G(d) minimum energy path (MEP) for the classical nitroaldol reaction. CCSD(T)/aug-cc-pVDZ//MP2/6-31+G(d) single-point energy calculations are in blue. MP2/6-31+G(d) energies are in parentheses. Relative energies without ZPE are in brackets. Energies are in kcal/mol. Bond lengths are in angstroms.

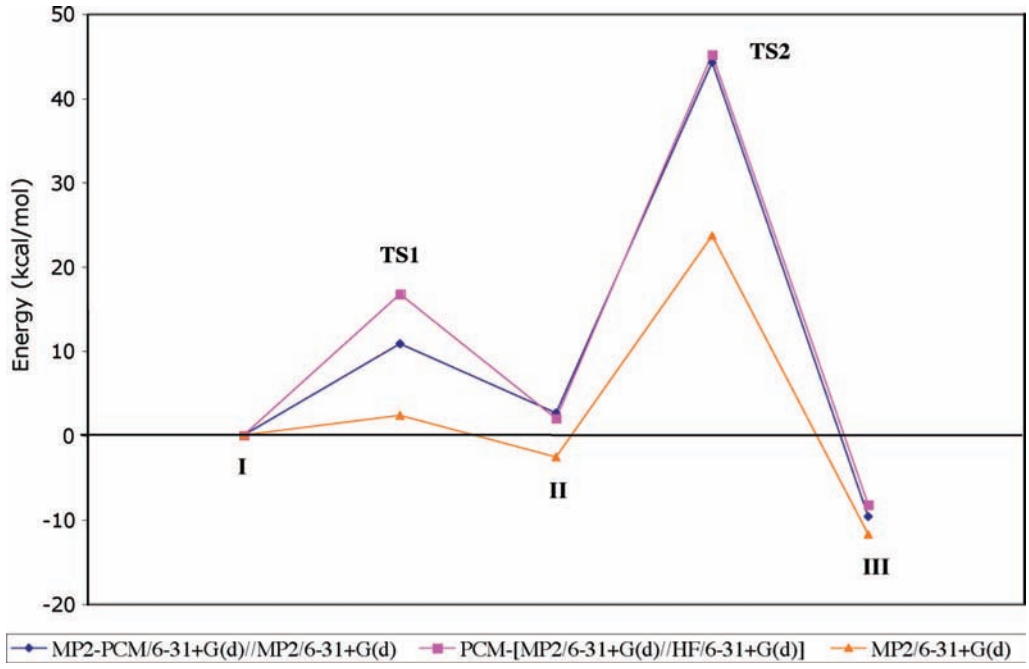

Figure 4. Solvent effects with PCM for the classical mechanism.

The step size used for the IRC calculations was 0.1 $(amu)^{1/2}$ bohr.[18,19] At the final MP2/6-31+G(d) geometries, improved relative energies and barriers were determined using singles and doubles coupled cluster theory with perturbative triples (CCSD(T)),[20,21] using the aug-cc-pVDZ[22] basis set. Partial charges on the optimized geometries were found using a Mulliken population analysis.[23] Solvent effects were taken into account with the polarizable continuum model (PCM)[24] using a solvent radius of 21.55 Å and a dielectric constant of 38.2 for nitromethane. PCM calculations were performed in two ways: in the first, PCM-MP2 single-point energies were performed at the MP2 gas-phase structures, and in the second, PCM-MP2 single-point energies were performed at the optimized geometries from PCM-HF. These two methods are denoted MP2-PCM/6-31+G(d)//MP2/6-31+G(d) and PCM-[MP2/6-31+G(d)//PCM-HF/6-31+G(d)], respectively. The relative energies of all minima and transition states include zero-point energy (ZPE) corrections, calculated from the MP2 frequencies. All QM calculations were done with GAMESS,[25,26] and MacMolPlt[27] was used to generate linear least motion (LLM) paths and to visualize all molecules.

III. Results and Discussion

The analysis of the nitroaldol reaction is presented in several subsections. In section III.1, the classical reaction is investigated by studying the mechanism for addition of deprotonated NO_2CH_3 to formaldehyde to yield a nitroalcohol **1** (Figure 2). A schematic of this mechanism is shown in Scheme 1. In section III.2, the effects of the solvent on the mechanism are taken into account in two ways: first by using the PCM continuum method and second by including an ab initio solvent molecule. In section III.3, the role of the amine catalyst is considered. The amine catalyst used by Huh et al. was an immobilized 3-[2-(aminoethylamino)ethylamino]propyl (AEP) group.[3] Methylamine is used in the present study as a model amine catalyst. The nonbonded effects of the methylamine catalyst were investigated by studying a mechanism in which a methylamine molecule is present as an observer; that is, this additional methylamine does not form covalent bonds to the reactants. In section III.4, three catalyzed mechanisms are investigated and compared; in these mechanisms covalent bonds are formed between the amine catalyst and formaldehyde (see Scheme 5). Structures are labeled in Figure 2. In section III.5 the effect of adding a second catalytic group to path D (Scheme 2) is considered. All mechanisms are compared to determine the most likely pathway(s) for the formation of the nitroalkene products in the gas phase.

III.1. Classical Reaction Mechanism. There are two steps in the classical mechanism (whose minimum energy path is shown in Figure 3): first, $(NO_2CH_2)^-$ adds to formaldehyde to form 2-nitroethoxide; in the second step a proton transfers to the carbonyl oxygen to form the 2-nitroethanol anion. In the following discussion, relative energies are quoted at the highest level of theory used: CCSD(T)/aug-cc-pVDZ//MP2/6-31+G(d). In Figure 3, structure **I**, the reactants formaldehyde and $(NO_2CH_2)^-$ form a van der Waals complex with a C−C bond length of 3.166 Å. In the first transition state (Figure 3, structure **TS1**) $(NO_2CH_2)^-$ attacks the carbonyl carbon forming a C−C bond giving 2-nitroethoxide (Figure 3, structure **II**). **TS1** has a stretched C−C distance of 2.291 Å and is 3.2 kcal/mol above complex **I**. Structure **II** is 1.4 kcal/mol lower in energy than the starting complex, **I**, and has a C−C bond length of 1.600 Å and an O−C−C angle of 109.3°.

Formation of 2-nitroethanol anion can proceed through a four-center transition state (Figure 3, structure **TS2**) in which a proton transfers from the carbon that is bonded to the NO_2 group to the carbonyl oxygen. **TS2** is 23.3 kcal/mol above the starting complex. This large barrier is due to the strain in the four-center transition state. In **TS2** The O−C−C angle is only 97.7°. The geometry of **5** is shown in Figure 3 structure **III**, which is 13.0 kcal/mol lower in energy than the starting complex and is a pseudocyclic compound with a hydrogen bond between the hydroxy group and an oxygen from nitromethane. The O−C−C bond angle has now opened to 113.8°.

MP2 Mulliken charges on the starting complex suggest that the nitromethane carbon has a charge of −0.53, and the nitro group caries a net charge of −0.78. The formaldehyde carbonyl carbon carries a small net negative charge of −0.04, and the

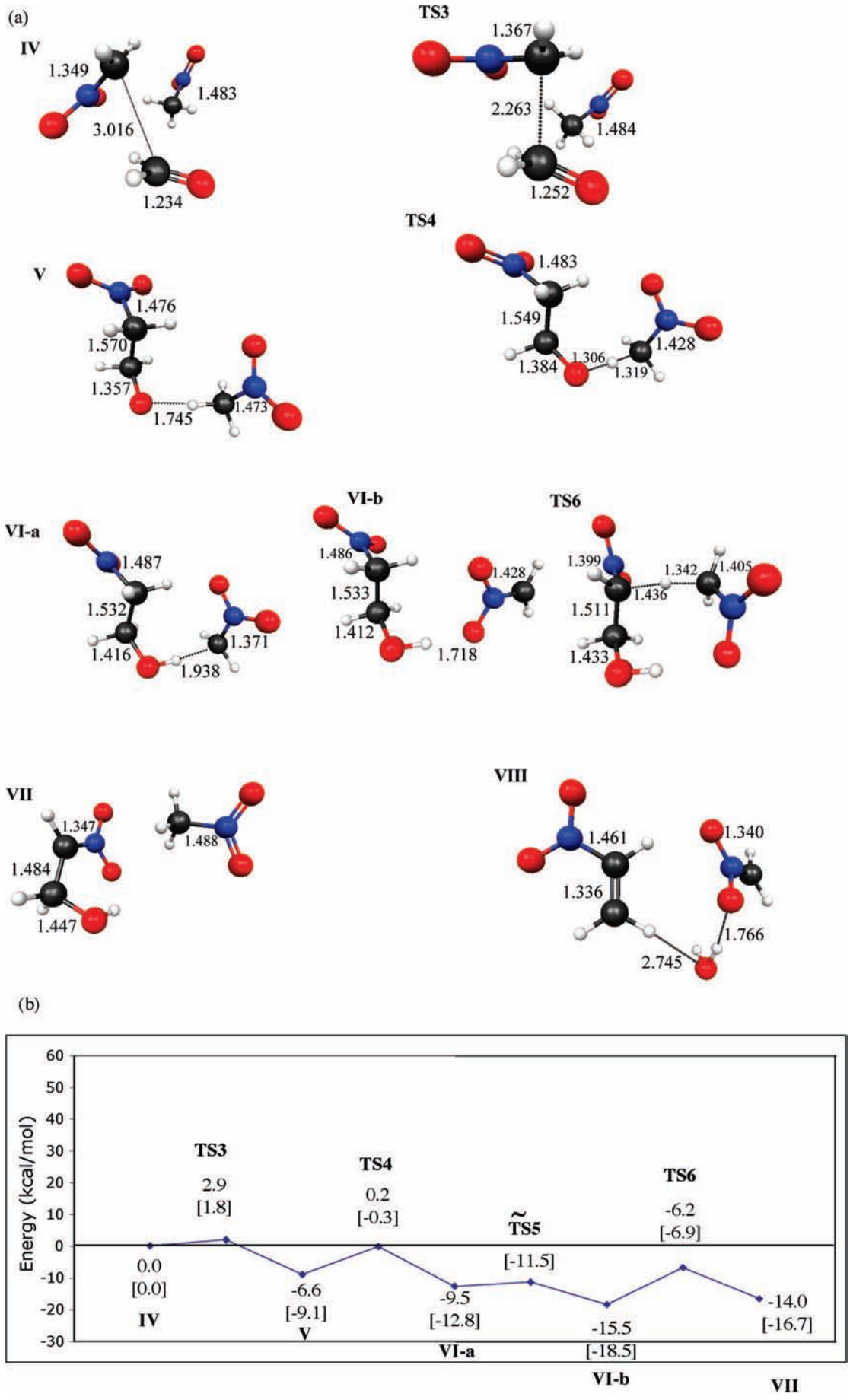

Figure 5. (a) MP2/6-31+G(d) reactants and products for classical nitroaldol reaction with ab initio solvent molecule. (b) Classical MP2/6-31+G(d) MEP. Relative energies without ZPE are in brackets. Energies are in kcal/mol. Bond lengths are in angstroms.

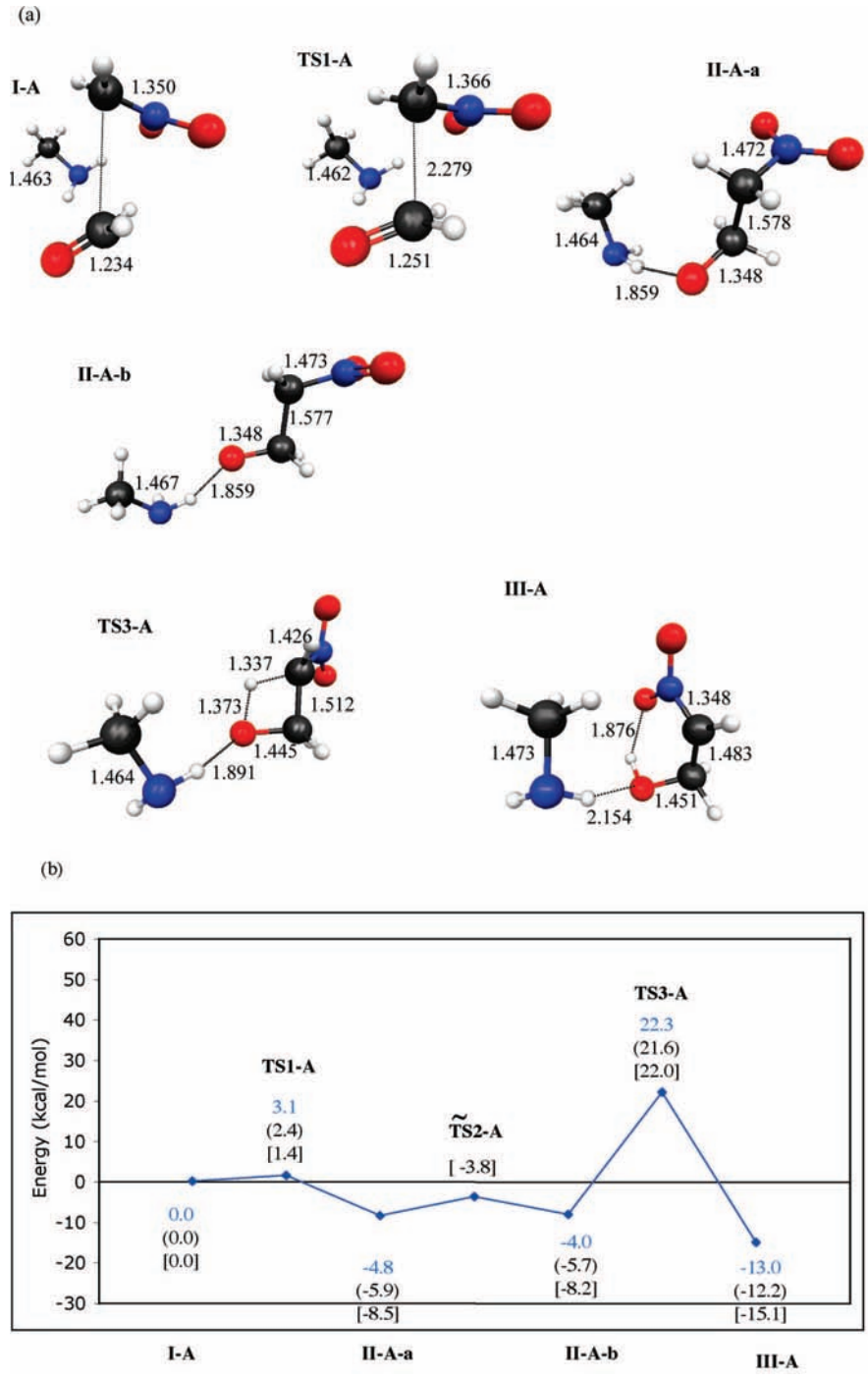

Figure 6. (a) MP2/6-31+G(d) minima and transition state structures for mechanism with an amine molecule present but not forming covalent bonds with reactants. (b) MP2/6-31+G(d) MEP. Relative energies without ZPE are in brackets. Energies are in kcal/mol. MP2/6-31+G(d) energies are in parentheses. Improved relative energies are from CCSD(T)/aug-cc-pVDZ//MP2/6-31+G(d) single-point energy calculations. Bond lengths are in angstroms.

carbonyl oxygen has a charge of −0.40. The charges do not change significantly from **I** to **II**. In **II**, the carbonyl oxygen has a net charge of −0.40, and the net negative charge on the nitro group is reduced slightly to −0.75. The Mulliken charges on **III** are significantly different from those in **I** or **II**. In **III** the nitromethane carbon has a charge of only −0.27, the carbonyl carbon has a charge of −0.22, the carbonyl oxygen has a charge of −0.74, and the nitro group has a net charge of −0.82. These values suggest significant charge delocalization in **III**.

The MP2/6-31+G(d) barrier at **TS1** reproduces the full core MP2 barrier determined by Lecea et al.[5] However, the MP3 and MP4SDQ barriers quoted by Lecea et al. are approximately twice as high as the CCSD(T)/aug-cc-pVDZ//MP2/6-31+G(d) values, indicating the unreliability of the MP3 and MP4SDQ energies. Lecea et al. did not report barriers for **TS2**. All MP2 relative energies and barrier heights in Figure 3 compare very well with those from CCSD(T)//MP2 single-point energy calculations.

III.2. Effects of the Nitromethane Solvent. Solvent effects for the classical mechanism were taken into account using the PCM continuum approach[24] for the nitromethane solvent, as illustrated in Figure 4. The dielectric constant chosen for the nitromethane solvent is the default GAMESS/PCM value of

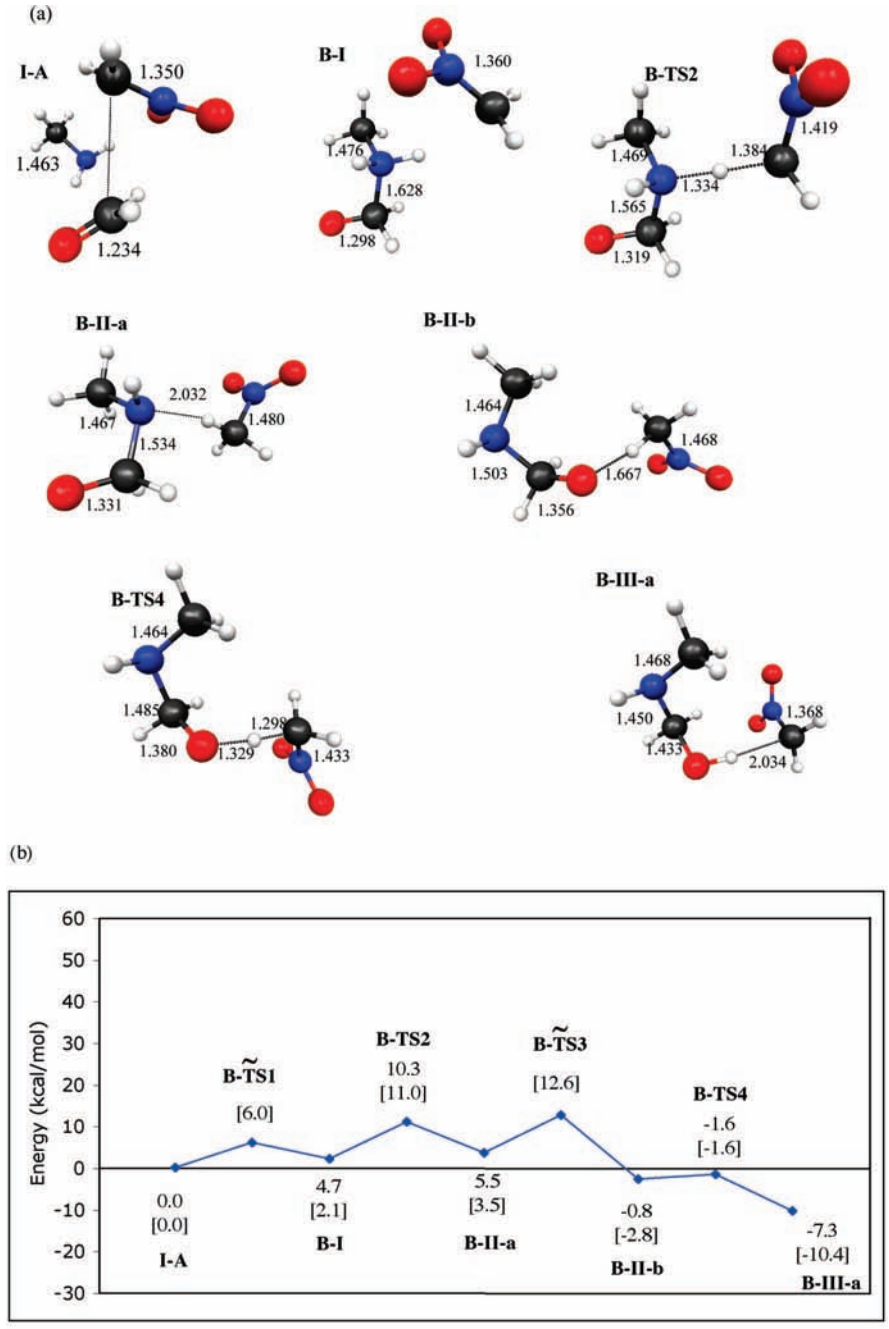

Figure 7. (a) MP2/6-31+G(d) minima and transition state structures for formation of **3**. (b) MP2/6-31+G(d) MEP. Relative energies without ZPE are in brackets. Energies are in kcal/mol. Bond lengths are in angstroms.

38.2.[25,26] Figure 4 shows a comparison of the MP2-PCM//MP2 and MP2-PCM//HF-PCM minimum energy paths. Both solvent approaches produce an increase in the **TS1** and **TS2** barrier heights relative to the gas-phase MP2 barriers. The **TS1** barrier is increased over the MP2 gas-phase barrier by 8.6 and 14.4 kcal/mol with MP2-PCM//MP2 and MP2-PCM//HF-PCM, respectively. The **TS2** barrier is raised by at least 20 kcal/mol with both PCM methods. PCM also slightly increases the energy of structure **II** relative to the starting structure as compared to the gas phase. When the PCM solvent is present, the Mulliken charge distribution is less delocalized than it is in the gas-phase species. For example, PCM increases the negative charge on the carbonyl oxygen in all species and decreases the amount of negative charge on the carbonyl carbon. To summarize, PCM has a minor effect on the predicted minima and transition state structures, differing in bond distances by less than 0.05 Å relative to the gas-phase Hartree−Fock values. Since the barrier heights in the presence of the PCM solvent are not reasonable, this method is not considered further.

Figure 5 demonstrates the effect of the addition of one ab initio solvent molecule to the classical mechanism. All resulting minima and transition states are shown in Figure 5a. The relative energies are presented in Figure 5b. A schematic of this mechanism is shown in Scheme 3. The first step of this mechanism is the addition of $(NO_2CH_2)^-$ to formaldehyde to form 2-nitroethoxide. Structure **5** is formed in two steps: First, a proton transfers from nitromethane to the carbonyl oxygen to form **4** and $(NO_2CH_2)^-$; then a proton transfers from the carbon bonded to the nitro group of **1** back to $(NO_2CH_2)^-$ to form nitromethane and **5**. **5** can now eliminate water to form the nitroethene products. The barrier height (2.9 kcal/mol) for addition of $(NO_2CH_2)^-$ to formaldehyde (Figure 5a, structure

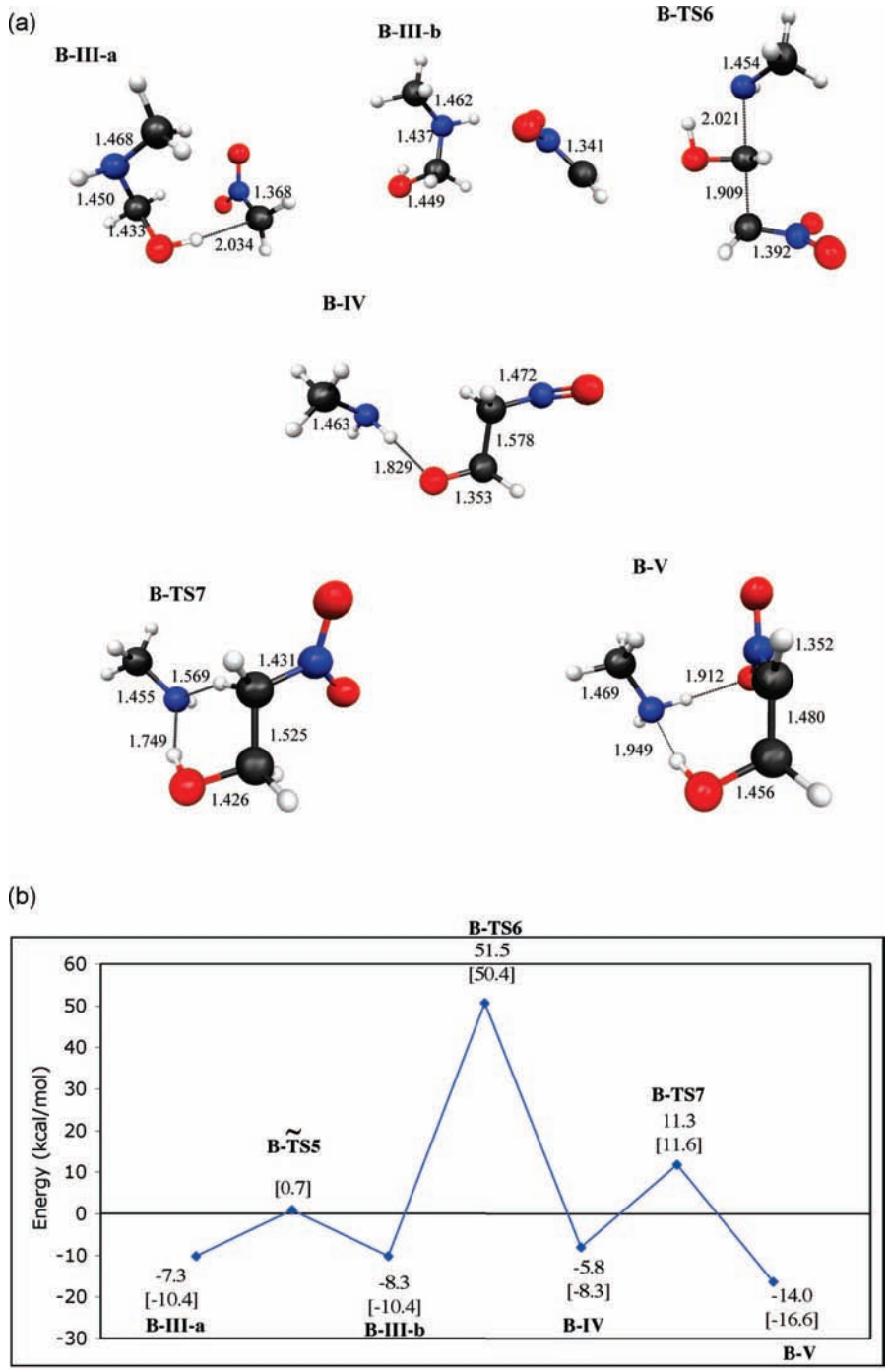

Figure 8. (a) MP2/6-31+G(d) minima and transition state structures for catalyzed mechanism pathway B. (b) MP2/6-31+G(d) MEP. The zero of energy corresponds to structure **I-A**. Relative energies without ZPE are in brackets. Energies are in kcal/mol. Bond lengths are in angstroms.

TS3) is virtually unchanged from the gas-phase value. Addition of an ab initio nitromethane solvent molecule can decrease the barrier for formation of 2-nitroethanol (cf., **TS2** in Figure 3) by using a two-step mechanism (Figure 5b). In the first step (Figure 5a, structure **TS4**) a proton transfers from nitromethane to the carbonyl oxygen of 2-nitroethoxide in structure **V** forming 2-nitroethanol and $(NO_2CH_2)^-$ (Figure 5a, structure **VI-a**). **TS4** is 6.8 kcal/mol higher in energy than **V**. In the second step of the nitroalcohol formation a proton on the carbon bonded to the nitro group of **1** needs to transfer to $(NO_2CH_2)^-$ to form 2-nitroethanol anion and nitromethane, but first isomer **VI-a** must convert to isomer **VI-b** (see Figure 5a). The barrier for this step (Figure 5b, $\widetilde{\mathbf{TS}}$ **5**) is estimated to be less than 1.3 kcal/mol higher in energy than **VI-a** by a series of constrained optimizations along an LLM path. The barrier for proton transfer to form 2-nitroethanol anion (Figure 5a, structure **TS6**) is 9.3 kcal/mol higher in energy than **VI-b** but still 6 kcal/mol below the starting reactants. The complex of **5** with nitromethane (Figure 5a, structure **VII**) is 14.0 kcal/mol lower in energy than the starting complex (see Figure 5b). The net energy requirement for formation of **5** in this mechanism is 2.9 kcal/mol, which is significantly lower than the net energy requirement in the classical mechanism (23.6 kcal/mol).

A transition state was not found for elimination of water from **VII** by proton transfer from a nitromethane solvent molecule. A series of constrained optimizations along an LLM path found an approximate upper bound of this barrier to be 37.8 kcal/mol higher in energy than the starting complex. The elimination

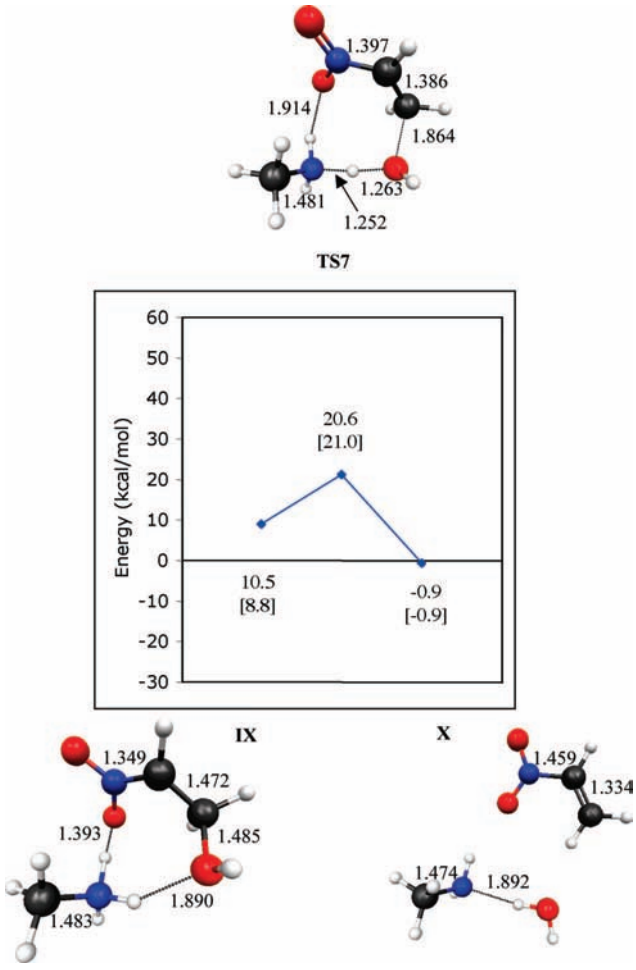

Figure 9. MP2/6-31+G(d) MEP for elimination of a nitroalcohol to give a nitroalkene. The zero of energy corresponds to the reactant complex of $CH_2O + CH_3NO_2 + CH_3NH_2$. Relative energies without ZPE are in brackets. Energies are in kcal/mol. Bond lengths are in angstroms.

product (Figure 2, structure **2**) is 4.5 kcal/mol lower in energy than the starting complex, and its geometry is shown in Figure 5a, structure **VIII**.

III.3. Nonbonded Effects of the Amine Catalyst. In the following mechanism (Figure 6), the nonbonded (environmental) effects of the methylamine catalyst were investigated. A schematic of this mechanism is shown in Scheme 4. In the first step $(NO_2CH_2)^-$ attacks the carbonyl carbon forming a C−C bond, producing **4**. A proton then transfers to the carbonyl oxygen to form **5**.

The minima and transition states for this mechanism are shown in Figure 6a, and the corresponding minimum energy path (MEP) is depicted in Figure 6b. **I-A** is a complex between formaldehyde, methylamine, and $(NO_2CH_2)^-$. In **I-A** there is no hydrogen bond between the complex of formaldehyde and $(NO_2CH_2)^-$. In **TS1-A**, $(NO_2CH_2)^-$ attacks the carbonyl carbon forming a C−C bond, leading to 2-nitroethoxide (Figure 6a, structure **II-A-a**). **TS1-A** is 3.1 kcal/mol higher in energy than the reactant complex (**I-A**), as shown in Figure 6b. **TS1-A** has a structure that is almost identical to the structure of **TS1** (see Figure 3), and their barrier heights are almost identical as well. In **TS1-A** there are no hydrogen bonds between CH_3NH_2 and the reacting molecules.

The next step in the mechanism is conversion from **II-A-a** to **II-A-b** (Figure 6b, $\widetilde{\text{TS}}$ **2-A**). In both **II-A-a** and structure **II-A-b**, there is a hydrogen bond between CH_3NH_2 and the carbonyl carbon, with H-bond lengths of 1.859 and 1.845 Å, respectively. The barrier for conversion from **II-A-a** to **II-A-b** (approximated by a series of optimizations along the LLM path) is less than 1 kcal/mol above **II-A-a**.

In the final step of this mechanism, structure **III-A** (Figure 6a) is formed. The transition state structure connecting **II-A-b** and **III-A** (Figure 6a, structure **TS3-A**) is a four-center transition state in which a proton transfers to the carbonyl oxygen. **TS3-A** is 22.3 kcal/mol higher in energy than the reactant complex. **TS3-A** has nearly the same geometry as the transition state in the classical mechanism, (Figure 3, structure **TS2**), and its barrier is only 1 kcal/mol lower in energy. The presence of CH_3NH_2 in a hydrogen-bonded arrangement causes no significant change in the bond lengths of **TS2** or **III** (Figure 3) with the addition of CH_3NH_2. The hydrogen-bond length involving CH_3NH_2 in **III-A** is 2.154 Å. To summarize, the presence of CH_3NH_2 does not significantly affect the barrier heights of the two transition states leading to the formation of 2-nitroethanol. Interaction with an ab initio solvent molecule as discussed in section III.2 is a much more effective way to lower the barrier height of the second transition state (Figure 3, structure **TS2**).

III.4. Catalysis Mechanisms. The mechanisms in which a covalent bond is formed between the catalyst and the reactants will now be discussed. A schematic of three possible catalyzed mechanisms is shown in Scheme 5. The first step in all catalyzed mechanisms is addition of methylamine to formaldehyde to form **3** (see Scheme 5a). Three possible pathways, arbitrarily labeled B, C, and D, are shown in Scheme 5b.

In path B, **3** undergoes an S_N2 reaction with $(NO_2CH_2)^-$ to form **4** and CH_3NH_2. A proton then transfers to the carbonyl oxygen to form **5**. Once a proton is added to the system, **5** can undergo elimination to form the nitroethene product, **2**. In Figure 3 path C, **3** (Figure 2) undergoes an S_N2 reaction with $(NO_2CH_2)^-$ to form **6**. In this path the leaving group is an hydroxide ion, rather than $(CH_3NH)^-$. A proton then transfers from the amine nitrogen of **6** to the hydroxide ion to form **7** and water. With the addition of a proton, the catalyst is regenerated and the nitroethene product, **2**, is formed. In Scheme 5 path D, water is eliminated from **3** by proton transfer from the amine nitrogen to the alcohol oxygen forming **8** and water. $(NO_2CH_2)^-$ can then add to the carbon of the imine double bond to form **7**. Once a proton is added to the system, the catalyst is regenerated and the nitroethene product, **2**, is formed.

***III.4.1. Formation of* 3.** The first step in the three catalyzed mechanisms is the formation of **3** (Scheme 5a). The minima and transition states for this step are shown in Figure 7a, and the corresponding MEP is shown in Figure 7b. In the first step, CH_3NH_2 adds to formaldehyde in **I-A** forming **B-I** (Figure 7b, **B-**$\widetilde{\text{TS}}$ **1**). A series of constrained optimizations along an LLM path was used to estimate the barrier height for this step. The upper bound for this barrier was found to be less than 1.3 kcal/mol higher in energy **I-A**. In the next step (Figure 7a, structure **B-TS2**) a proton transfers from the amine nitrogen to $(NO_2CH_2)^-$ to form isomer **B-II-a**. **B-TS2** is 5.6 kcal/mol above **B-I**, and **B-II-a** is 5.5 kcal/mol higher in energy than the reactants. After inversion of the amine nitrogen in isomer **B-II-a** to form isomer **B-II-b** (Figure 7b, **B-**$\widetilde{\text{TS}}$ **3**) a proton can now transfer to the carbonyl carbon (Figure 7a, structure **B-TS4**) to form **B-III-a** (Figure 7a). The barrier for inversion of the amine and rotation of the hydroxy group was estimated by a series of constrained optimizations on an LLM path. The transition state structure for the proton transfer is **B-TS4**. **B-TS4** was found to be −0.8 kcal/mol lower in energy than **B-II-b** after ZPE was included.

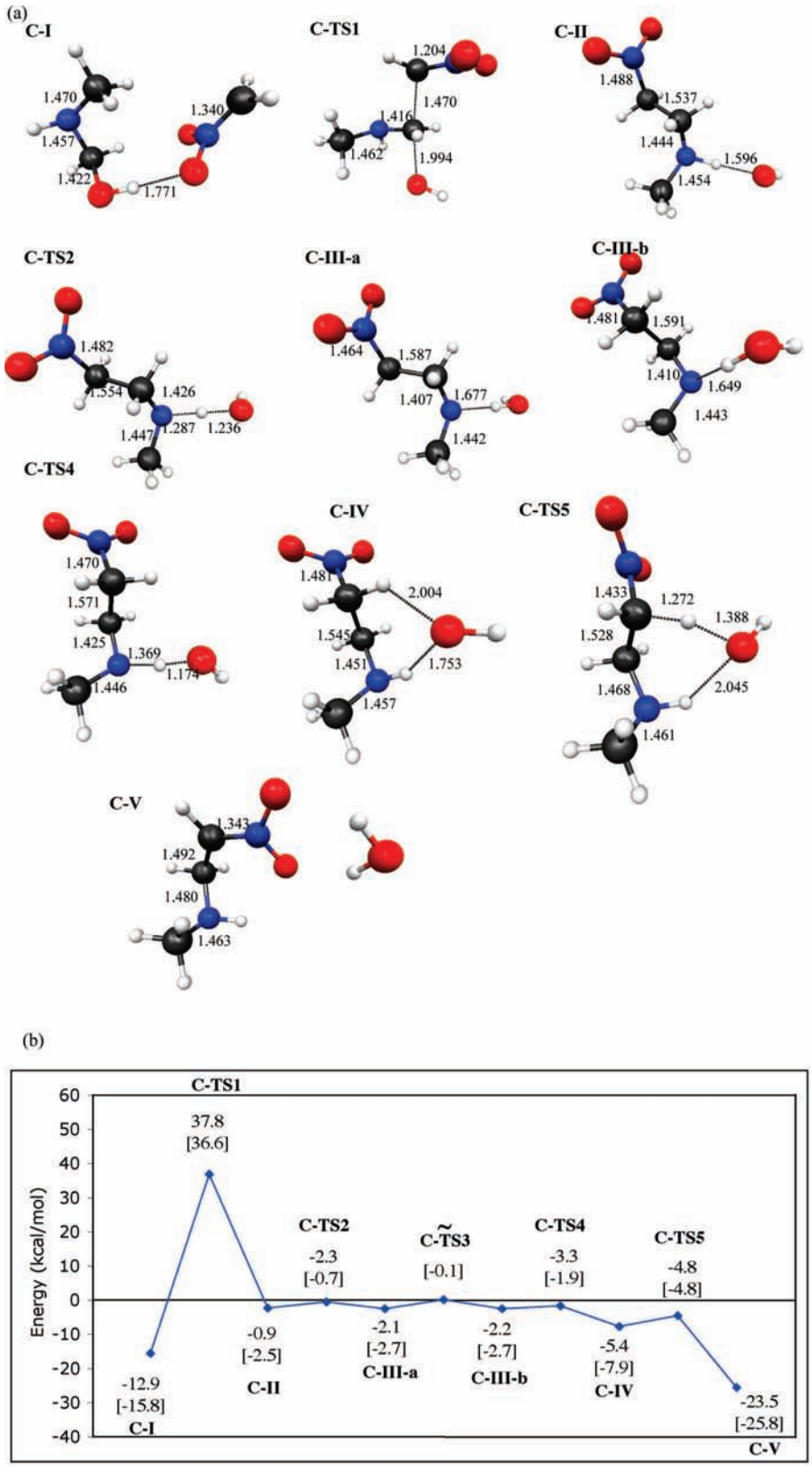

Figure 10. (a) MP2/6-31+G(d) minima and transition states in catalyzed mechanism pathway C. (b) MP2/6-31+G(d) MEP. The zero of energy corresponds to structure **I-A**. Relative energies without ZPE are in brackets. Energies are in kcal/mol. Bond lengths are in angstroms.

III.4.2. Catalyzed Mechanism: Path B. The MEP for path B (see Scheme 5b and associated discussion) is shown in Figure 8. The first step in this mechanism is the conversion of **B-III-a** to **B-III-b**. This step is simply a rotation of methylaminomethanol with respect to $(NO_2CH_2)^-$. The barrier was approximated by a series of constrained optimizations along an LLM path. The upper bound for this step is 9.7 kcal/mol above **I-A** (Figure 8, $\tilde{\mathbf{TS}}$ **5**). The second step in this catalyzed mechanism path is attack of the carbonyl carbon in structure **B-III-b** by $(NO_2CH_2)^-$ to form the nitroalkoxide and regenerate the catalyst (Figure 8a, structure **B-IV**). The transition state for this step is **B-TS6**, which is 51.5 kcal/mol higher in energy than **I-A**. In this step

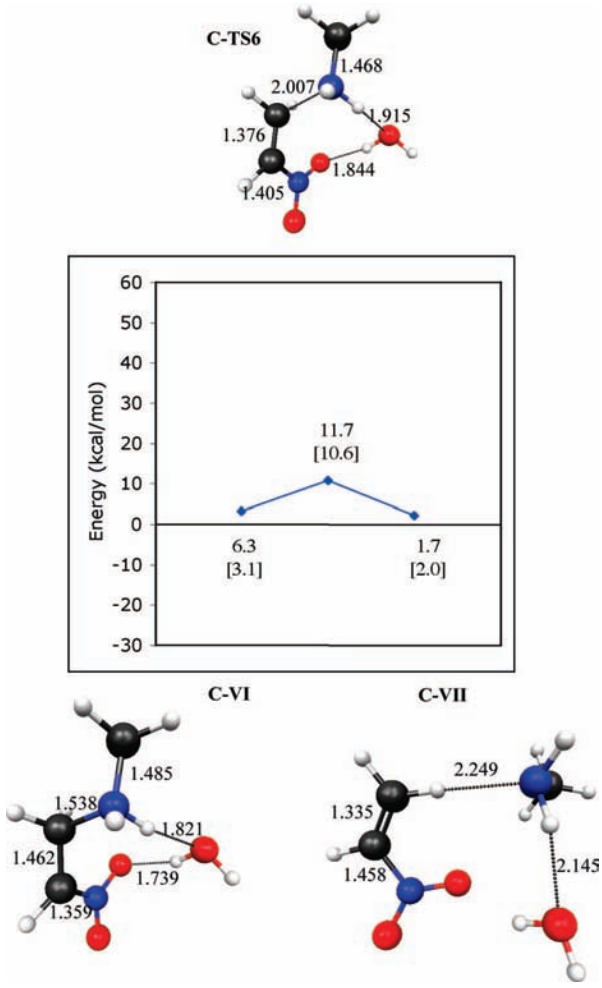

Figure 11. MP2/6-31+G(d) MEP for regeneration of amine catalyst in catalyzed mechanism pathway D. The zero of energy corresponds to the reactant complex of $CH_2O + CH_3NO_2 + CH_3NH_2$. Relative energies without ZPE are in brackets. Energies are in kcal/mol. Bond lengths are in angstroms.

$(NO_2CH_2)^-$ first attacks the carbonyl carbon eliminating $(CH_3NH)^-$, along with a simultaneous proton transfer from the alcohol to the amine nitrogen. **B-V** is 14.0 kcal/mol below the reactants.

In order to form **B-V** from **B-IV**, a proton must transfer from the carbon bonded to the NO_2 group to the carbonyl oxygen. During the investigation of the classical mechanism, the MP2/6-31+G(d) barrier for this step with no methylamine catalyst group (Figure 3, structure **TS2**) was found to be 23.6 kcal/mol higher in energy than the reactant complex (Figure 3, structure **I**). When the methylamine catalyst forms covalent bonds with the reactants the barrier for proton transfer drops to only 11.3 kcal/mol (Figure 8a, structure **B-TS7**) above the reactant complex. **B-TS7** is 10.3 kcal/mol lower in energy than **TS3-A**. This is because adding a methylamine transforms the four-center transition state (Figure 6a, structure **TS3-A**) to a six-center transition state (Figure 8a, structure **B-TS7**). In the four-center transition state the proton transfers directly from the carbon bonded to the nitro group to the carbonyl oxygen. In the six-center transition state (**B-TS7**), a proton transfers from CH_3NH_2 to the carbonyl alcohol, and then in the same step, a proton transfers from the carbon bonded to NO_2 back to CH_3NH. Such mechanism modifications are well-known, especially when water molecules are present. This was especially true for the synthesis of three- and four-membered cyclosiloxanes,[28] where the potential energy barriers are reduced nearly to zero in the presence of a water molecule. The O−C−C bond angle in **B-TS7** is 108.4°, which is less strained than in **TS2** (Figure 3).

After a proton has been added to the system **B-V** becomes **IX** (Figure 9). **IX** can undergo dehydration as shown in Figure 9 to give the final nitroalkene product (Figure 2, structure **2**). This step occurs by a concerted reaction in which a protonated amine donates a proton to the hydroxy group in **IX** (Figure 9). The transition state for elimination of water (Figure 9, structure **TS7**) is 20.6 kcal/mol higher in energy than the reactant complex of $CH_2O + CH_3NO_2 + CH_3NH_2$. The product (Figure 9, structure **X**) is −0.9 kcal/mol lower in energy than the reactant complex. In **TS7**, the distance between the alcohol carbon and the alcohol oxygen elongates to 1.864 Å as a proton transfers to the carbonyl oxygen. The distance between the proton transferring from $CH_3NH_3^+$ and the alcohol oxygen is 1.252 Å.

III.4.3. Catalyzed Mechanism: Path C. The second option for the catalyzed mechanism is depicted in Scheme 5b path C. The minima and transition states in path C are shown in Figure 10a, and the corresponding MEP is shown in Figure 10b. The starting complex for path B is structure **C-I** (Figure 10a), which is a complex of methylaminemethanol with $(NO_2CH_2)^-$. The transition state for the first step along this path is structure **C-TS1** (Figure 10a). **C-TS1** is 37.8 kcal/mol higher in energy than **I-A** (Figure 10b). **C-II** is 0.9 kcal/mol lower in energy than the reactant complex, **I-A**. **C-TS1** is a pentacoordinated transition state, in which $(NO_2CH_2)^-$ adds as the nucleophile and HO^- is the leaving group, in an S_N2-like process. In structure **C-II**, the amine hydrogen is hydrogen-bonded to the OH oxygen.

A proton can now transfer from the amine nitrogen of **C-II** OH^- to form **C-III-a** (Figure 10a), in which water is H-bonded to the amine N. The transition state for this step is structure **C-TS2** (Figure 10a). Before ZPE is accounted for, this transition state is 1.7 kcal/mol higher in energy than **C-II**; however, with ZPE included, the energy of C-TS2 is 1.4 kcal/mol *lower* in energy than **C-II**, indicating that **C-TS2** is not a true TS on the potential energy surface (PES). **C-III-a** is 2.1 kcal/mol lower in energy than **C-I**. The barrier for the conversion of **C-III-a** to **C-III-b** (∼2.6 kcal/mol for rotation of the water molecule) was approximated by a series of constrained optimizations along an LLM path.

From **C-III-b**, a proton on the carbon bonded to the nitro group must transfer to the amine nitrogen. This is a two-step process (Figure 10a **C-TS4** and **C-TS5**) in which a proton is first transferred from the water molecule to the amine nitrogen and then a second proton is transferred from the carbon bonded to the nitro group back to the hydroxide ion. Including ZPE, the barriers for both **C-TS4** and **C-TS5** are lower in energy than **C-III-a**. At this point, structure **C-IV** is 23.5 kcal/mol lower in energy than the reactants. In the final step of path C (Figure 11) a proton is added to the system and nitromethane is regenerated forming **2** (Figure 11, **C-VII**). The transition state for this step is **C-TS5** has a barrier 11.7 kcal/mol above the net-neutral complex of the reactants.

III.4.4. Catalyzed Mechanism: Path D. The third pathway for the catalyzed mechanism is shown in Scheme 5b, path D. The reactants and transition states along pathway D are shown in Figure 12a, and the corresponding MEP is shown in Figure 12b. In the first step of this mechanism (Figure 12a, structure **D-TS1**), a proton transfers from the amine nitrogen of **D-I** to the carbon to form nitromethane **D-II-a** (Figure 12, parts a and b). **D-TS1** is 10.9 kcal/mol higher in energy than **D-I**.

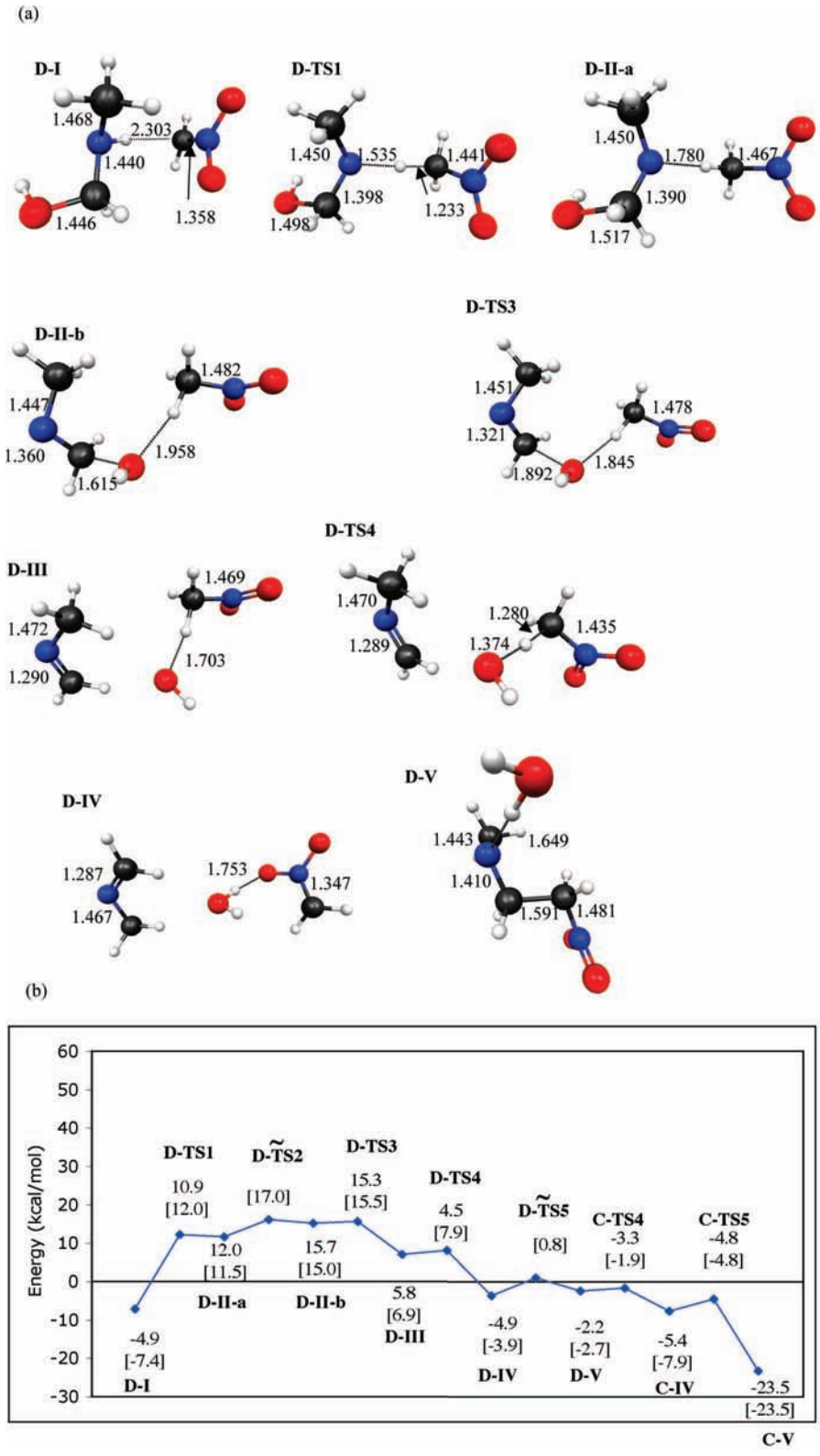

Figure 12. (a) MP2/6-31+G(d) minima and transition states for catalyzed mechanism pathway D. (b) MP2/6-31+G(d) MEP. The zero of energy corresponds to structure **I-A**. Relative energies without ZPE are in brackets. Energies are in kcal/mol. Bond lengths are in angstroms.

D-II-a must now convert to **D-II-b**. The barrier for this step (Figure 12b, **D-$\widetilde{\text{TS}}$ 2**) was approximated by a series of constrained optimizations along an LLM path to be less than 2.0 kcal/mol.

In the next step (Figure 12a, structure **D-TS3**), a proton transfers from nitromethane to the alcohol oxygen and a hydroxy group is eliminated forming **D-III**. **D-TS3** is higher in energy than **D-II-b** before ZPE is accounted for. When the ZPE is included, the energy of the transition state is 0.4 kcal/mol lower in energy than **D-II-b**. Water is formed when a proton is transferred from nitromethane to the hydroxy group (Figure 12a, structure **D-TS4**). **D-TS4** is higher in energy than **D-III** before the ZPE is included, but after the ZPE is added in, the transition state is 1.3 kcal/mol below **D-III**.

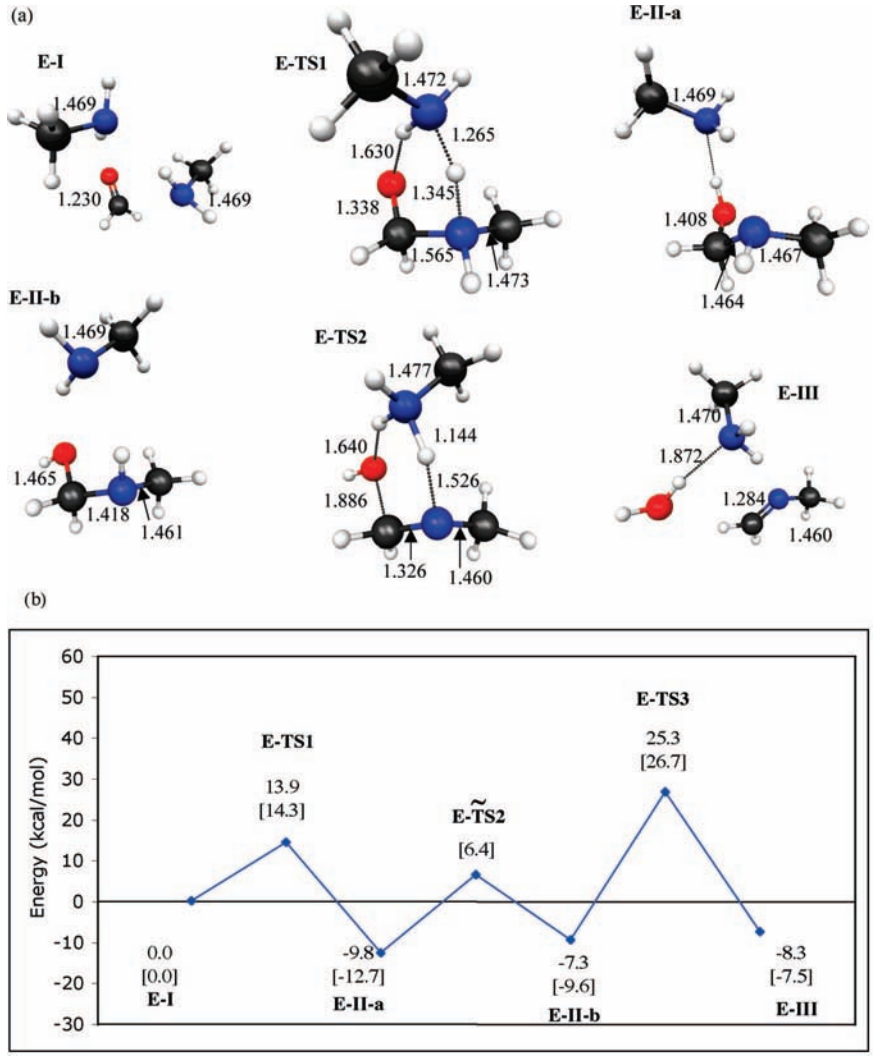

Figure 13. (a) MP2/6-31+G(d) minima and transition states for imine formation with an additional methylamine, (b) MP2/6-31+G(d) MEP. Relative energies without ZPE are in brackets. Energies are in kcal/mol. Bond lengths are in angstroms.

Now that water has been eliminated, nitromethane anion can add to the carbon of the C−N double bond to form a C−C single bond. The transition state for this step is **D-$\widetilde{\text{TS}}$ 5** (Figure 12b). The barrier for this step is simply the barrier for moving the water molecule out of the way, making the imine available to attack by $(NO_2CH_2)^-$. This barrier is approximated by a series of constrained optimizations on an LLM path to be less than 2 kcal/mol. A proton can now transfer to form the β-nitroamine in the same way as in mechanism C (see **C-TS4** and **C-TS5** in Figure 10a).

In summary, only path D has a net energy requirement (7 kcal/mol) less than that of the classical mechanism. Paths B and C can be eliminated because of their high barriers compared to those in the classical catalyzed mechanism and path D of the catalyzed mechanism. The S_N2 reaction in these paths would be especially difficult if a more complex and possibly sterically hindered aldehyde was used. Catalyzed mechanism D has the lowest barriers of any mechanism that was investigated here.

III.5. Multiple Amine Molecules. In the mechanism proposed by Demicheli et al.[4] (Scheme 2), the intermediates formed are the same as in Scheme 5, path D, except that multiple amine catalyst groups are proposed to be involved. This could be an important effect. To investigate this, a second methylamine molecule was added to the reaction of formaldehyde with methylamine. A schematic of this mechanism is shown in Scheme 6. The first step is addition of methylamine to formaldehyde to eliminate water and form **8**. $(NO_2CH_2)^-$ then adds to the carbon of the imine C−N double bond to form **7**. In the final step acid is added and the catalyst is regenerated forming the product, **2**.

The effect of adding a second methylamine molecule will be investigated in two steps: first, the energy requirement for imine formation will be presented; then, the net energy requirement for addition of $(NO_2CH_2)^-$ to the imine and the regeneration of the methylamine catalyst will be explored.

III.5.1. Imine Formation. The structures of the minima and transition states for imine formation are shown in Figure 13a, and the corresponding MEP is shown in Figure 13b. The starting complex in this mechanism is formaldehyde plus two methylamine molecules (Figure 13a, structure **E-I**). The first step in this mechanism is the addition of nitromethane to formaldehyde (Figure 13a, structure **E-TS1**). In this step, the amine attacks the carbonyl carbon, and at the same time a proton transfers to the to the second amine. Then, a proton transfers from the second amine to the carbonyl oxygen forming **E-II-a**. **E-TS1** has a barrier of 13.9 kcal/mol (Figure 13a). In **E-II-a**, there is a hydrogen bond between the alcohol and the methylamine.

Before water can be eliminated, the amine nitrogen in **E-II-a** (Figure 13a) must undergo inversion to make the proton available to CH_3NH_2. This also breaks the O−H···N hydrogen

bond. The barrier for conversion from **E-II-a** to **E-II-b** (Figure 13, **E-$\widetilde{TS}$ 2**) is estimated to be less than 6.4 kcal/mol higher in energy than **E-II-a**. Water can now be eliminated with a barrier of 25.3 kcal/mol to form the imine (Figure 13a, structure **E-III**). The net energy requirement of 25.3 kcal/mol for this first step is already much higher than that for path D discussed above, so this mechanism that involves two methylamine molecules is not likely to be competitive. Although the second part of this mechanism, addition of NO_2CH_2 and regeneration of the catalyst, has been explored in detail, it is not presented here to save space.

IV. Conclusions

Several pathways for the nitroaldol reaction have been compared to determine the energetically most favorable mechanism. To form the final nitroalkene products, the reaction must pass through either a 2-nitroethanol or an imine intermediate. The highest barrier (23.6 kcal/mol) in the classical mechanism is for the formation of 2-nitroethanol (Figure 3, structure **III**). Addition of solvent effects represented by PCM increases this barrier by 20 kcal/mol. When an ab initio solvent molecule is added, the net energy requirement of nitroalkene formation is reduced to less than 2.9 kcal/mol. The decrease in the barrier height is due to a change from a one-step mechanism with a strained four-center transition state to a two-step mechanism that involves a six-center transition state. Effectively, the solvent molecule serves a role of a catalyst in this manner.

Once the nitroalcohol is formed it can undergo elimination by forming a six-center transition state with the methylamine catalyst. The barrier for elimination is very high unless the amine catalyst is present. The net energy requirement for this "classical" mechanism is 20.6 kcal/mol. In an alternative mechanism, first methylaminomethanol is formed, then water is eliminated forming an imine intermediate, and finally the catalyst is regenerated. Then net energy requirement for this mechanism is 17.0 kcal/mol, which is only 3.6 kcal/mol lower in energy than the "classical" mechanism, indicating that neither mechanism can be eliminated as a possibility. When a second amine is added to the system the net energy requirement actually increases, demonstrating that a second amine molecule is not necessary to facilitate the reaction. Solvent effects were shown to be very important for nitroalcohol formation; however, PCM does not give a realistic representation of the implicit solvent effects. Future work will investigate the effect of the silica pore and explicit observer solvent molecules. Since transfers of hydrogen atoms are implicated in the mechanisms explored here, the importance of quantum effects on these motions must also be explored.

Acknowledgment. This research was supported by a Grant from the U.S. Department of Energy to the Ames Laboratory, office of BES, under contract DE-AC02-07CH11358.

References and Notes

(1) Henry, L. *C. R. Hebd. Seances Acad. Sci.* **1895**, *120*, 1265.

(2) Rosini, G. In *Comprehensive Organic Synthesis*; Trost, B. M., Fleming, I., Heathcock, C. H., Eds.; Pergamon: Oxford, 1991; pp 321−340.

(3) Huh, S.; Chen, H.-T.; Wiench, J. W.; Pruski, M.; Lin, V. S.-Y. *J. Am. Chem. Soc.* **2004**, *126*, 1010.

(4) Demicheli, G.; Maggi, R.; Mazzacani, A.; Righi, P.; Sartori, G.; Bigi, F. *Tetrahedron Lett.* **2001**, *42*, 2401.

(5) Lecea, B.; Arrieta, A.; Morao, I.; Cossío, F. P. *Chem. Eur. J.* **1997**, *3*, 20.

(6) Krishnan, R.; Pople, J. A. *Int. J. Quantum Chem.* **1978**, *14*, 91.

(7) Beksic, D.; Bertran, J.; Lluch, J. M.; Hynes, J. T. *J. Phys. Chem. A* **1998**, *102*, 3977.

(8) Hall, N. E.; Smith, B. J. *J. Phys. Chem. A* **1998**, *102*, 4930.

(9) Curtiss, J. A.; Ragahavachari, K.; Pople, J. A. *J. Chem. Phys.* **1993**, *98*, 1293.

(10) Møller, C.; Plesset, M. S. *Phys. Rev.* **1934**, *46*, 618.

(11) Fletcher, G. D.; Rendell, A. P.; Sherwood, P. *Mol. Phys.* **1997**, *91*, 431.

(12) Hehre, W. J.; Ditchfield, R.; Pople, J. A. *J. Chem. Phys.* **1972**, *56*, 2257.

(13) Hariharan, P. C.; Pople, J. A. *Theor. Chem. Acta* **1973**, *28*, 213.

(14) Gordon, M. S. *Chem. Phys. Lett.* **1980**, *76*, 163.

(15) Clark, T.; Chandrasekhar, J.; Spitznagel, G. W.; Schleyer, P. v. R. *J. Comput. Chem.* **1983**, *4*, 294.

(16) Gonzalez, C.; Schlegel, H. B. *J. Phys. Chem.* **1990**, *94*, 5523.

(17) Gonzalez, C.; Schlegel, H. B. *J. Phys. Chem.* **1991**, *95*, 5853.

(18) Garrett, B. C.; Redmon, M. J.; Steckler, R.; Truhlar, D. G.; Baldridge, K. K.; Bartol, D.; Schmidt, M. W.; Gordon, M. S. *J. Phys. Chem.* **1988**, *92*, 1476.

(19) Truhlar, D. G.; Gordon, M. S. *Science* **1990**, *249*, 491.

(20) Raghavachari, K.; Trucks, G. W.; Pople, J. A.; Head-Gordon, M. *Chem. Phys. Lett.* **1989**, *157*, 479.

(21) Piecuch, P.; Kucharski, S. A.; Kowalski, K.; Musial, M. *Comput. Phys. Commun.* **2000**, *149*, 71.

(22) Dunning, T. H., Jr. *J. Chem. Phys.* **1989**, *90*, 1007.

(23) Mulliken, R. S. *J. Chem. Phys.* **1955**, *23*, 1833–1840.

(24) Miertus, S.; Scrocco, E.; Tomasi, J. *Chem. Phys.* **1981**, *55*, 117.

(25) Schmidt, M. W.; Baldridge, K. K.; Boatz, J. A.; Elbert, S. T.; Gordon, M. S.; Jensen, J. H.; Koseki, S.; Matsunaga, N.; Nguyen, K. A.; Su, S. J.; Windus, T. L.; Dupuis, M.; Montgomery, J. A. *J. Comput. Chem.* **1993**, *14*, 1347.

(26) Schmidt, M. W.; Gordon, M. S. In *Theory and Applications of Computational Chemistry: The First Forty Years*; Dykstra, C. E., Frenking, G., Kim, K. S., Scuseria, G. E., Eds.; Elsevier: New York, 2005; pp 1167−1189.

(27) Bode, B. M.; Gordon, M. S. *J. Mol. Graphics Modell.* **1999**, *16*, 133.

(28) Kudo, T.; Gordon, M. S. *J. Phys. Chem. A* **2000**, *104*, 4058.

JP805135P